Spatiotemporal instabilities in dispersive nonlinear media

L. W. Liou
The Institute of Optics, University of Rochester, Rochester, New York 14627

X. D. Cao and C. J. McKinstrie
Department of Mechanical Engineering, University of Rochester, Rochester, New York 14627

Govind P. Agrawal
The Institute of Optics, University of Rochester, Rochester, New York 14627
(Received 3 June 1992)

A spatiotemporal instability is shown to occur in a dispersive nonlinear optical medium whose refractive index varies linearly with the optical intensity (the Kerr medium). The physical origin of the spatiotemporal instability lies in the simultaneous presence of diffraction and dispersion in nonlinear media. For a self-focusing medium the instability can occur for both normal and anomalous dispersion. In contrast, the instability exists only in the normal-dispersion region of a self-defocusing medium. A linear stability analysis is used to predict the initial growth rate of the spatiotemporal instability. Numerical simulations are used to analyze the behavior in the nonlinear regime where the results of the linear stability analysis become invalid. Our results show that the spatiotemporally modulated mode has a larger growth rate than that of the spatially homogeneous mode and is expected to dominate in practice. The periodic state eventually evolves into spatiotemporal chaos with further propagation inside the nonlinear medium.

PACS number(s): 42.65.Jx, 42.60.Fc, 42.65.Re

I. INTRODUCTION

Instabilities and chaos can occur in many types of nonlinear physical systems belonging to plasma physics [1–3], fluid mechanics [4,5], and nonlinear optics [6–11]. Generally speaking, optical instabilities can be classified as temporal or spatial depending on whether light is modulated temporally or spatially after its passage through the nonlinear medium. A temporal instability which has attracted considerable attention, known as the modulation instability [4,12,13], occurs through an interplay between self-phase-modulation and group-velocity dispersion. It manifests itself as the breakup of continuous-wave (cw) or quasi-cw radiation into a train of ultrashort pulses when light propagates in a self-focusing medium with anomalous dispersion [12]. Its spatial analog corresponds to the development of a ring pattern on the transverse intensity profile of a cw beam in a self-focusing medium [14,15]. The role played by anomalous dispersion in the case of temporal modulation instability is taken on by diffraction in the case of spatial instability. In this paper we study a spatio-temporal instability occurring when both diffraction and dispersion are present simultaneously. This spatiotemporal instability is of fundamental importance as it shows how diffraction and dispersion act together to couple space and time. While this instability has previously been studied in the context of plasma physics [1–3] and hydrodynamics [4,5], it has attracted little attention in the field of nonlinear optics, where it can be used to convert a cw or quasi-cw beam into a train of ultrashort pulses by spatially modulating the amplitude or phase of the optical beam. We use numerical simulations to discuss the feasibility of such a practical application.

This paper is organized as follows. The basic propagation equation is presented in Sec. II by considering both diffraction and dispersion in a nonlinear medium. The linear stability analysis is carried out in Sec. III where the gain curves for the spatiotemporal modulation instability are presented. Section IV extends the linear stability analysis of Sec. III in the nonlinear regime by solving the wave equation numerically. Finally, the results are discussed and summarized in Sec. V.

II. WAVE PROPAGATION IN DISPERSIVE NONLINEAR MEDIA

For simplicity of discussion, we consider the simplest kind of nonlinearity corresponding to the so-called Kerr medium whose refractive index varies linearly with the optical intensity, i.e.,

$$\tilde{n}(\omega,I)=n(\omega)+n_2 I \ , \tag{1}$$

where ω is the optical frequency, $n(\omega)$ is the linear part of the refractive index, I is the optical intensity, and n_2 is the nonlinearity parameter related to the third-order nonlinear susceptibility [13]. In general, n_2 is also frequency dependent. However, in many practical situations, it varies little over the frequency range of interest and can be treated as constant. Chromatic dispersion is then included through the frequency dependence of $n(\omega)$. Optical instabilities in Kerr media have been studied before [16–18]. In most of the earlier work, however, the Kerr medium is assumed to be nondispersive. We show here

that new instabilities can occur when the dispersive nature of the Kerr medium is considered.

Wave propagation in a dispersive nonlinear medium is governed by Maxwell's equations together with Eq. (1). To simplify the analysis, we solve the problem by making the slowly-varying-envelope and paraxial approximations and write the electric field as

$$\mathbf{E}(\mathbf{r},t)=\mathrm{Re}\{\hat{\mathbf{e}}A(\mathbf{r},t)\exp[i(\beta_0 z-\omega_0 t)]\}\ , \tag{2}$$

where Re stands for the real part, $\hat{\mathbf{e}}$ is the polarization unit vector assumed to remain unchanged during beam propagation, $A(\mathbf{r},t)$ is the envelope assumed to vary slowly with respect to both z and t, ω_0 is the carrier frequency, and $\beta_0=n(\omega_0)\omega_0/c$ is the propagation constant. The slowly varying amplitude $A(\mathbf{r},t)$ satisfies the following paraxial wave equation [19]:

$$i\left[\frac{\partial A}{\partial z}+\frac{1}{v_g}\frac{\partial A}{\partial t}\right]+\frac{1}{2\beta_0}\left[\frac{\partial^2 A}{\partial x^2}+\frac{\partial^2 A}{\partial y^2}\right]-\frac{\beta_2}{2}\frac{\partial^2 A}{\partial t^2}+\frac{\beta_0 n_2}{n_0}|A|^2A=0\ , \tag{3}$$

where v_g is the group velocity, β_2 is the group-velocity dispersion parameter (in the notation of Ref. [13]), and $n_0=n(\omega_0)$ is the linear refractive index. The parameter $\beta_2=(d^2\beta/d\omega^2)_{\omega=\omega_0}$ with $\beta=n(\omega)\omega/c$. Both β_2 and n_2 can be positive or negative. The dispersion is said to be normal or anomalous depending on whether β_2 is positive or negative. The nonlinear medium is said to be self-focusing or self-defocusing depending on whether n_2 is positive or negative. The character of spatiotemporal instability discussed here changes considerably with the relative signs of β_2 and n_2; this will become clear later.

III. SPATIOTEMPORAL INSTABILITY

In general, Eq. (3) should be solved numerically. The origin of spatiotemporal instability, however, can be understood by considering the ideal case of a cw plane wave having a constant amplitude $\sqrt{I_0}$, (I_0 is proportional to the beam intensity) at the input end of the nonlinear medium. Equation (3) can be solved analytically in that case since A is independent of x, y, and t. The solution is

$$A(x,y,z,t)=\sqrt{I_0}\exp(i\gamma z)\ , \tag{4}$$

where

$$\gamma=\frac{\beta_0 n_2}{n_0}I_0=\frac{2\pi}{\lambda}n_2 I_0\ . \tag{5}$$

and λ is the wavelength of incident light. Equation (4) shows that the cw plane wave remains unchanged during propagation except for acquiring an intensity-dependent phase shift.

Stability of the steady-state solution, Eq. (4), depends on whether small perturbations grow or decay with propagation. We use the standard linear stability analysis [13] and assume that A is perturbed slightly such that

$$A(x,y,z,t)=[\sqrt{I_0}+a(x,y,z,t)]\exp(i\gamma z)\ , \tag{6}$$

where the perturbation $|a|\ll\sqrt{I_0}$. By substituting Eq. (6) in Eq. (3) and linearizing in a, we obtain

$$i\left[\frac{\partial a}{\partial z}+\frac{1}{v_g}\frac{\partial a}{\partial t}\right]+\frac{1}{2\beta_0}\left[\frac{\partial^2 a}{\partial x^2}+\frac{\partial^2 a}{\partial y^2}\right]-\frac{\beta_2}{2}\frac{\partial^2 a}{\partial t^2}+\gamma(a+a^*)=0\ . \tag{7}$$

This linear equation can be solved analytically. If we assume a general plane wave solution of the form

$$a=a_1\cos[\mathbf{K}\cdot\mathbf{r}-\Omega(t-z/v_g)]+ia_2\sin[\mathbf{K}\cdot\mathbf{r}-\Omega(t-z/v_g)]\ , \tag{8}$$

a nontrivial solution is found to exist only when the wave vector $\mathbf{K}$ and the frequency Ω satisfy the following dispersion relation:

$$4\beta_0^2K_z^2=(K_x^2+K_y^2-\beta_0\beta_2\Omega^2)(K_x^2+K_y^2-\beta_0\beta_2\Omega^2-4\gamma\beta_0)\ , \tag{9}$$

where K_x, K_y and K_z are the Cartesian components of $\mathbf{K}$. This dispersion relation reduces to that obtained for modulation instability in optical fibers [13] in the limit $K_x=K_y=0$ (diffraction absent due to the guided nature of the optical field). The steady-state solution becomes unstable whenever K_z has a negative imaginary part since the perturbation then grows exponentially with the intensity gain given by $g=2\,\mathrm{Im}(K_z)$. In general, g is a function of K_x, K_y, and Ω. However, g depends on K_x and K_y only through $K_s=(K_x^2+K_y^2)^{1/2}$. Thus g can be treated as a function of K_s and Ω only. It is useful to introduce a spatial frequency Ω_s as

$$\Omega_s=\frac{K_s}{\sqrt{\beta_0|\beta_2|}}=\left[\frac{K_x^2+K_y^2}{\beta_0|\beta_2|}\right]^{1/2}\ . \tag{10}$$

By using Eq. (9), the gain can be written in the form

$$g(\Omega,\Omega_s)=|\beta_2|[\Omega_s^2-\mathrm{sgn}(\beta_2)\Omega^2]^{1/2}\times[\mathrm{sgn}(n_2)\Omega_c^2+\mathrm{sgn}(\beta_2)\Omega^2-\Omega_s^2]^{1/2}\ , \tag{11}$$

where

$$\Omega_c^2=\frac{4|\gamma|}{|\beta_2|}=\frac{8\pi|n_2|I_0}{\lambda|\beta_2|}\ . \tag{12}$$

Equation (11) shows that perturbation at a temporal frequency Ω and a spatial frequency Ω_s would grow exponentially due to an inherent instability of the steady-state solution. We call this instability a spatiotemporal instability because it leads to simultaneous spatial and temporal modulations of the steady state. The range of Ω and Ω_s over which instability occurs depends on the relative signs of n_2 and β_2. It is easy to see that no instability occurs when both n_2 and β_2 are negative. For the three remaining choices of the combinations of signs for n_2 and β_2, there exists some range of Ω and Ω_s for which the gain is real and positive. Figure 1 shows the instability region in the (Ω,Ω_s) plane for the three cases. The

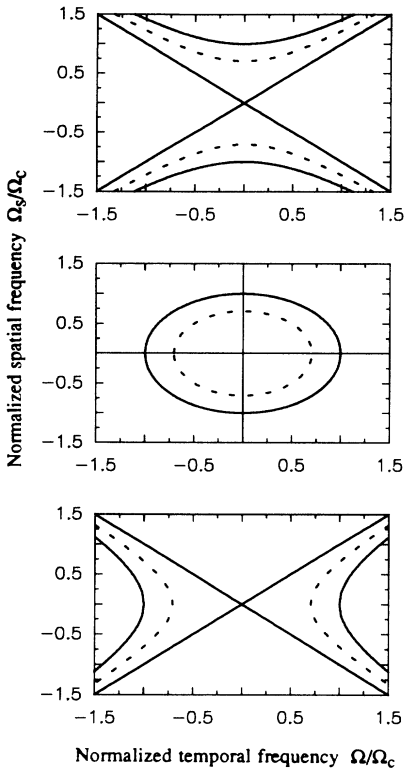

FIG. 1. Ranges of normalized temporal frequency Ω/Ω_c (horizontal axis) and normalized spatial frequency Ω_s/Ω_c (vertical axis) for which the spatiotemporal instability occurs for the three cases: (a) $n_2>0$, $\beta_2>0$; (b) $n_2>0$, $\beta_2<0$; (c) $n_2<0$, $\beta_2>0$. Solid lines enclosing the instability region are contours of zero gain. Dashed line in each case indicates the contour of maximum gain.

dashed line in each case shows the contour of maximum gain, whereas solid lines show the contours of zero gain.

Several interesting conclusions can be drawn from Fig. 1. In the absence of diffraction ($\Omega_s=0$), the spatiotemporal instability reduces to the temporal modulation instability observed in optical fibers [12,13] and occurs only when $n_2>0$ and $\beta_2<0$ [Fig. 1(b)]. This instability is preserved even in the presence of diffraction, but now temporal modulation can be accompanied by spatial modulation as long as $\Omega^2+\Omega_s^2<\Omega_c^2$. The most interesting feature is that the spatiotemporal instability does not necessarily require anomalous dispersion. It can occur even in the normal dispersion regime of a self-focusing medium ($n_2>0,\beta_2>0$), although the instability domain is quite different [Fig. 1(a)]. Indeed, the instability gain occurs for all frequencies Ω such that

$$\Omega_s^2-\Omega_c^2\le\Omega^2\le\Omega_s^2 . \tag{13}$$

Spatial modulation at Ω_s would thus lead to temporal modulation at the frequency Ω for which the gain is maximum. The same situation exists in the normal dispersion region of a self-defocusing medium [Fig. 1(c)] except that Ω is now bounded in the range

$$\Omega_s^2\le\Omega^2\le\Omega_s^2+\Omega_c^2 . \tag{14}$$

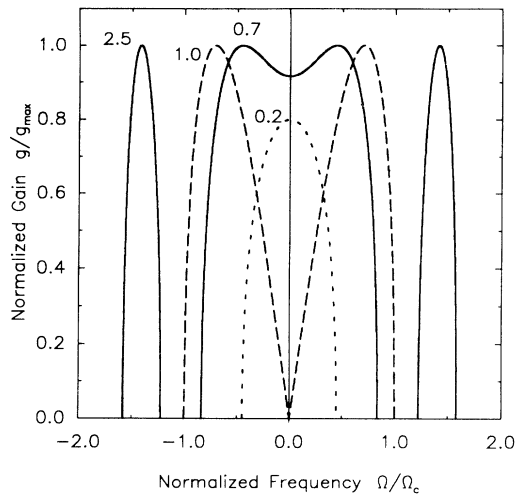

FIG. 2. Normalized gain plotted as a function of the normalized temporal frequency Ω/Ω_c for four values of Ω_s^2/Ω_c^2 for the case of a self-focusing medium with normal dispersion ($n_2>0$, $\beta_2>0$). Self-pulsing occurs only for $\Omega_s>\Omega_c/\sqrt{2}$.

In both cases cw light can be converted into a train of ultrashort pulses as a result of the spatiotemporal instability described in this paper by simply imposing a spatial modulation on the input beam. The case of self-defocusing is most interesting since the repetition rate Ω can be made quite large by increasing Ω_s and Ω_c (i.e., by increasing the intensity of the input cw beam).

Figures 2 and 3 show the variation of instability gain g with Ω/Ω_c for several values of Ω_s/Ω_c by using Eq. (11) in the normal dispersion region ($\beta_2>0$) of self-focusing and self-defocusing media, respectively. In the self-focusing case, the gain exists for all values of $\Omega_s>0$. The gain peak is located at $\Omega=0$ for $\Omega_s<\Omega_c/\sqrt{2}$ and shifts away from it for larger values of Ω_s. Physically, the tem-

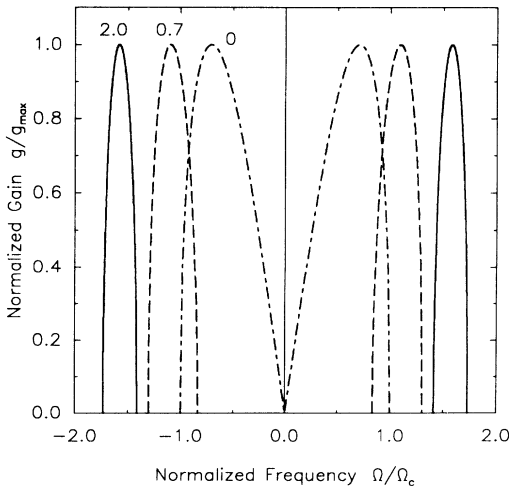

FIG. 3. Same as in Fig. 2 except that the nonlinear medium is self-defocusing ($n_2<0$). In this case self-pulsing occurs for all values of Ω_s.

poral modulation would be induced only when Ω_s exceeds $\Omega_c/\sqrt{2}$. By contrast, in the self-defocusing case, spatial modulation induces temporal modulation for all values of Ω_s. In each case the gain is normalized to its peak value $g_{\max}$ given by

$$g_{\max}=\frac{|\beta_2|\Omega_c^2}{2}=\frac{4\pi|n_2|I_0}{\lambda} . \tag{15}$$

The maximum gain is seen to be twice the nonlinear phase shift as given in Eq. (5) and is entirely determined by the wavelength and the nonlinear index change $\Delta n_{\rm NL}=|n_2|I_0$. In the visible region ($\lambda\sim 0.5\ \mu$m), the instability gain exceeds 20 cm^{-1} even for $\Delta n_{\rm NL}=10^{-4}$. In order for the instability to develop from noise [12], the nonlinear medium should be long enough to amplify the perturbation by a factor of 10^7 or so. Since $\exp(gL)=10^7$ for $gL\approx 16.1$, the spatiotemporal instability can be observed in a nonlinear medium of length $L<1$ cm when $\Delta n_{\rm NL}$ exceeds 10^{-4}. The required intensity depends on the value of $|n_2|$.

IV. NUMERICAL SIMULATIONS

The linear stability analysis detailed above indicates the possibility of producing a pulse train through the spatial modulation of a cw beam. However, the analysis is limited in scope simply because the exponential growth of perturbations ceases to occur when the perturbation amplitude becomes comparable to that of the incident beam. A numerical analysis of the evolution of spatiotemporal instability beyond the applicability of the linear analysis becomes necessary in the nonlinear regime.

We present the numerical solutions to Eq. (3) corresponding to the case of normal dispersion in a self-defocusing medium ($n_2<0,\beta_2>0$). Exact solutions are difficult to obtain even with supercomputers because of the four-dimensional nature of the problem. For simplicity, the diffractive effects are limited to one transverse dimension. Although, strictly speaking, the results are only valid for wave propagation in planar waveguides, they may indicate the qualitative behavior even for bulk media. For numerical calculations, Eq. (3) is normalized to the form

$$i\frac{\partial U}{\partial\xi}+\frac{1}{2}\frac{\partial^2 U}{\partial\eta^2}-\frac{1}{2}\frac{\partial^2 U}{\partial\tau^2}+|U|^2U=0 \tag{16}$$

by using the following normalized variables:

$$\xi=\gamma' z\ ,\quad \eta=\sqrt{\gamma'\beta_0}x,$$
$$\tau=\sqrt{\gamma'/|\beta_2|}\left[t-\frac{z}{v_g}\right]\ ,\quad U=\frac{A}{\sqrt{I'}}\ , \tag{17}$$

where $\gamma'=\gamma I'/I_0$ and I' is an intensity used for normalization.

Equation (16) is solved numerically, utilizing the split-step Fourier method [20]. The initial field distribution at the entrance to the nonlinear medium is a sinusoidally modulated plane wave $U=U_0[1+a_2\sin(f_s\eta)]$ with $a_s=0.1$ and $f_s=2U_0\Omega_s/\Omega_c$. From Fig. 3, it can be concluded that in the absence of any applied spatial modulation, temporal instability can develop at the normalized temporal frequency $f_1=2U_0\Omega_1/\Omega_c$ with a gain of $g_{\max}$, where Ω_1 corresponds to the peak of the gain curve for $\Omega_s=0$ in Fig. 3, i.e., $\Omega_1/\Omega_c=1/\sqrt{2}$ and $f_1=\sqrt{2}U_0$. When the cw plane wave is spatially modulated at f_s, the figure indicates that there will be a corresponding normalized temporal frequency, denoted here by f_2, that likewise exhibits a gain of $g_{\max}$. Thus the linear theory shows that the two temporal frequencies f_1 and f_2 have the same growth rate. However, the growth rates can be quite different in the nonlinear regime due to mode competition. The purpose of numerical simulations is to identify which frequency wins the nonlinear mode competition. In a laboratory experiment, noise in the system provides the seed from which temporal frequencies begin to develop. However, for the numerical simulations, it is necessary to explicitly provide an initial seed at the temporal frequency f_1, f_2, or both to stimulate a response (induced modulation instability). To examine the subtle effects of the applied perturbing frequencies in the numerical simulations, the results of different initial temporal frequency seedings are considered below.

The spatial modulation is applied at the normalized frequency $f_s=13$. The corresponding induced temporal frequency which has a peak in the gain curve near $f_2=14$ is provided with an initial amplitude seeding of 0.005. Thus the input field has the form

$$U(\xi=0,\eta,\tau)=U_0[1+0.1\sin(f_s\eta)][1+0.005\sin(f_2\tau)]\ , \tag{18}$$

where the amplitude U_0 is taken to be 5. Figure 4 shows the temporal and spectral distribution of the field intensity at $\eta=0$ at a propagation distance of $\xi=0.25$ ($z=12.5/g_{\max}$) into the medium. The dotted curve, shown for comparison, is the input field intensity at $\xi=0$. The linear theory predicts that the frequency f_1 should evolve simultaneously and at the same rate as f_2. However, since no seed was provided at that frequency, only the frequency f_2 grows until it generates higher harmon-

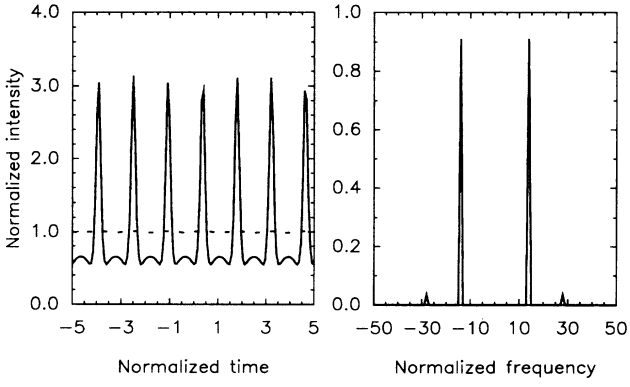

FIG. 4. Temporal and spectral distribution of optical intensity at a propagation distance $\xi=0.25$ with initial seeding at $f_2=14$ [see Eq. (18)]. The dotted curve shows the input intensity distribution. The input cw beam is modulated sinusoidally such that $f_s=14$.

ics through nonlinear interactions within the medium as seen in Fig. 4. Since f_2 is the dominant spectral component, the spatiotemporal instability gives rise to a periodic modulation at a repetition rate of f_2. We refer to this case as the spatially inhomogeneous (SI) case since temporal modulations are accompanied by spatial modulations.

When f_1 is applied as the only temporal frequency seed to the input cw beam, we would expect the spatially homogeneous (SH) mode ($f_2=0, f_1=\sqrt{2}U_0\approx 7$) to dominate the power spectrum for the same reason that the f_2 frequency component dominated in the preceding case. This is indeed the situation, as shown in Fig. 5, where the temporal and spectral distributions are shown under conditions identical to those of Fig. 4. An interesting point to note is that even though the initial perturbation amplitude of the SI mode (5×10^{-4} at $f_s=13, f_2=14$) is smaller by an order of magnitude than that of the SH mode (5×10^{-3} at $f_s=0 f_1=7$), the SI mode grows much more rapidly than the SH mode in the nonlinear regime beyond the applicability of the linear stability analysis. For this reason, the depth of modulation is much larger than that of the SH mode, given the same amount of time for the instability to develop. It is remarkable that the gain of the SI mode is much larger than that of the SH mode in the nonlinear region despite the linear theory prediction that these two frequency components would initially grow at the same exponential rate.

In a practical situation the SI and SH modes would evolve simultaneously and their growth rates would be affected through their mutual nonlinear interaction. To include such a nonlinear coupling we consider the case in which both frequencies f_1 and f_2 are initially seeded. Then the input field takes the form

$$U(\xi=0,\eta,\tau)=U_0[1+0.1\sin(f_s\eta)] \times[1+0.005\sin(f_1\tau)+0.005\sin(f_2\tau)] . \quad (19)$$

Figure 6 shows the temporal distribution of the field intensity and the corresponding power spectrum under conditions identical to those of Figs. 4 and 5. In order to show the multiline nature of the power spectrum clearly, the vertical axis of the spectrum plots the normalized amplitude. In spite of the smaller initial perturbation amplitude of the SI mode, it dominates the power spectrum through the frequency components at f_2 and its harmonics. In fact, the power contained in the f_2 frequency component exceeds that of the f_1 component as early as $\xi=0.05$. The spectral asymmetry seen in Fig. 6 appears to be a consequence of the fact that f_1 and f_2 are multiples of each other ($f_2=2f_1$). In the nonlinear regime new frequency components at harmonics of f_1 and f_2 and at $f_1\pm f_2$ are expected to be generated. Several of these components overlap and induce a strong coupling between the SI and SH modes. This coupling not only makes the spectrum asymmetric but also gives rise to the temporal distribution seen in the figure.

In the preceding simulation, f_2 is a multiple of f_1. To analyze the situation where f_1 and f_2 are incommensurate, the value of f_s is taken to be 15; the corresponding temporal frequency at the gain peak is located near $f_2=17$. Figure 7 shows the temporal and spectral behavior at the same propagation distance as in Fig. 6. The

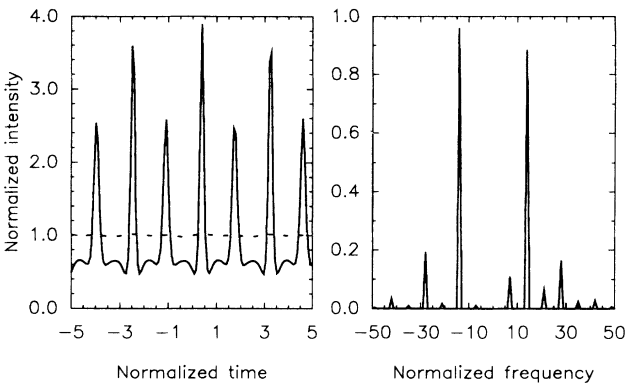

FIG. 6. Same as in Fig. 4 except the initial seed is supplied at both frequencies $f_1=7$ and $f_2=14$ [see Eq. (19)]. Normalized amplitude is plotted on the vertical axis of the spectrum to show multiple peaks clearly.

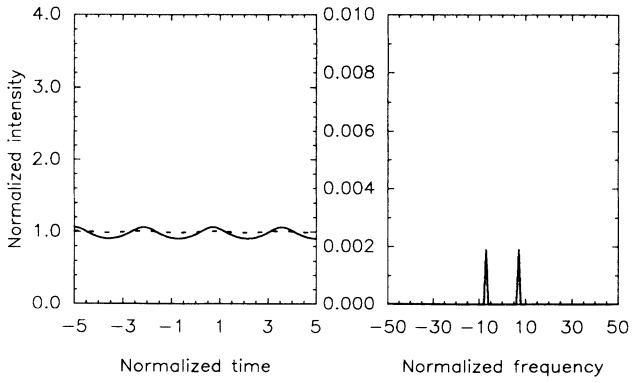

FIG. 5. Same as in Fig. 4 except the initial seeding is at $f_1=7$.

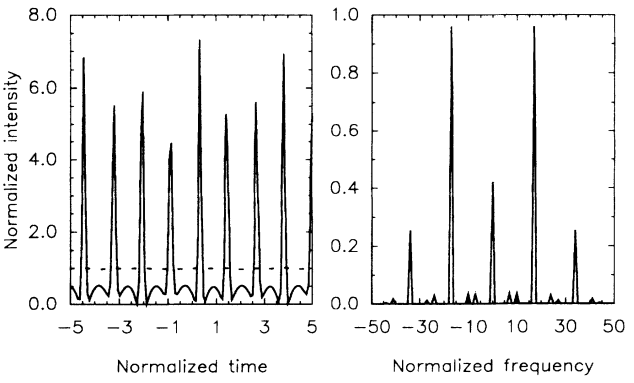

FIG. 7. Same as in Fig. 6 except $f_2=17$ and the spatial frequency $f_s=15$. The propagation distance is $\xi=0.25$.

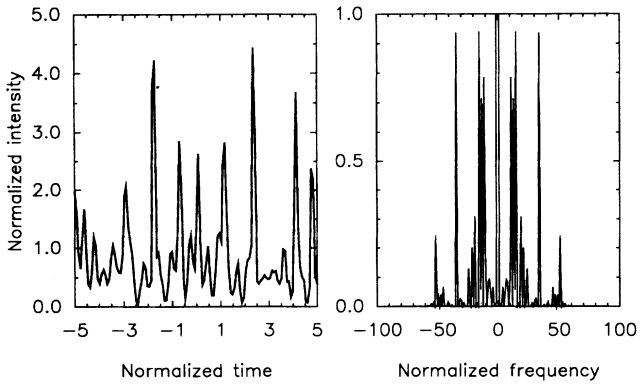

FIG. 8. Same as in Fig. 7 except the propagation distance is $\xi=0.35$.

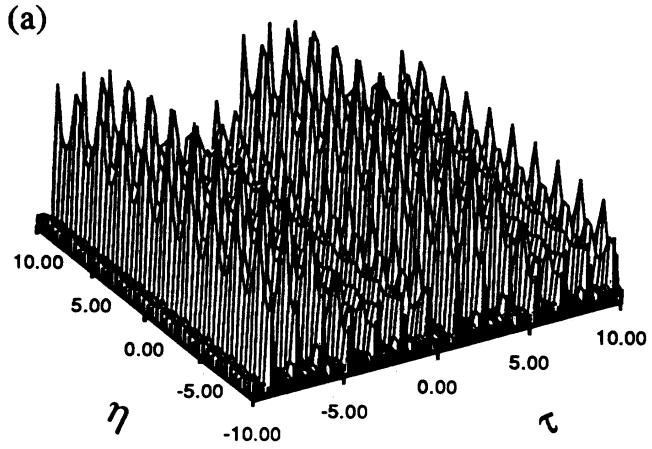

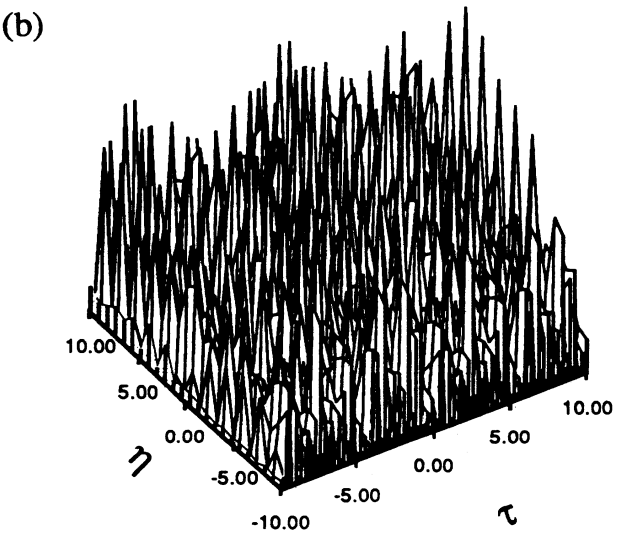

FIG. 9. Field intensity as a function of both the transverse spatial coordinate and time at normalized propagation distances of $\xi=0.3$ and 0.5.

most notable feature is the dominance of the spectrum by f_2 and its harmonics (corresponding to the SI mode). The SH mode does not grow significantly as little power is carried by the spectral components at f_1 and its harmonics. The nonlinear generation of other frequency components such as f_2-f_1 is also kept to a minimum. Figure 7 shows that the depth of modulation can approach 100% with a proper selection of the spatial frequency at the input. The zero-frequency (dc) component in the power spectrum is due to the residual cw background. Since the cw background in Figs. 4–6 is several times larger than in this case, the dc component was not shown in those spectral plots. With further propagation, frequency components arising from nonlinear processes such as sum and difference frequency generation and four-wave mixing acquire significant power levels, resulting in a chaotic output. An example of chaos is shown in Fig. 8, which corresponds to a propagation distance of $\xi=0.35$.

The intensity distributions and power spectra displayed in Figs. 4–8 are shown for a fixed transverse position in space $\eta=0$. However, the spatiotemporal nature of the instability can be more clearly seen in a three-dimensional plot of the field intensity as a function of both space and time. Figure 9 shows such a plot at propagation distances of $\xi=0.3$ and 0.5 where the only applied temporal frequency seed is f_2 (same as in Fig. 4). Figure 9(a) corresponds to $\xi=0.3$, a distance slightly greater than that of Fig. 4. Here we clearly see the spatiotemporal nature of the instability induced by imposing a spatial modulation. Figure 9(b) shows the situation at twice the propagation distance of Fig. 4 ($\xi=0.5$). It indicates that the periodic state eventually degenerates into spatiotemporal chaos.

V. DISCUSSION AND CONCLUSIONS

A spatiotemporal instability is shown to occur in a dispersive Kerr medium as a result of interplay among diffraction, dispersion, and self-phase modulation. In the case of self-focusing, the instability can occur both for normal and anomalous dispersion. In contrast, the instability exists only in the normal dispersion region of a self-defocusing medium. In the latter case, numerical simulations incorporating one transverse dimension demonstrate that temporal modulations can be induced on a laser beam by imposing a spatial intensity modulation on the input cw beam. The temporal period of these modulations can be controlled through the period of the spatial modulation and can be much shorter than that occurring in the absence of spatial intensity modulation. Given enough time to develop, the periodic modulation usually degenerates into spatiotemporal chaos. From the standpoint of the underlying nonlinear dynamics, more work is required to understand the transition from self-pulsing to chaos quantitatively.

One may expect a qualitatively similar behavior for the case of a self-focusing medium with normal dispersion. This situation is particularly interesting since the medium is temporally stable in the absence of spatial modulations.

Numerical simulations suggest that even though temporal modulations can be induced by imposing spatial modulation, the temporal modulation depth is much smaller than that obtained in the self-defocusing case.

The experimental observations of spatiotemporal instabilities would be of considerable interest. An atomic vapor such as sodium can be used for this purpose. Other possibilities consist of using either a nonlinear organic polymer or glasses doped with semiconductors or other suitable nonlinear material.

ACKNOWLEDGMENTS

The authors thank R. W. Boyd for discussions. The research is supported in part by the National Science Foundation (Grants Nos. ECS-9010599 and PHY-9057093).

[1] A. G. Litvak, in *Reviews of Plasma Physics,* edited by M. A. Leontovich (Consultants Bureau, New York, 1986), Vol. 10, and references therein.
[2] C. J. McKinstrie and G. G. Luther, Phys. Scr. **T30**, 31 (1990), and references therein.
[3] A. G. Litvak, T. A. Petrova, A. M. Sergeev, and A. D. Yunakovskii, Fiz. Plazmy **9**, 495 (1983). [Sov. J. Plasma Phys. **9**, 287 (1983)].
[4] A. Davey and K. Stewartson, Proc. R. Soc. London Ser. A **338**, 101 (1974).
[5] H. C. Yuen and B. M. Lake, Adv. Appl. Mech. **22**, 67 (1982), and references therein.
[6] *Optical Instabilities,* edited by R. W. Boyd, M. G. Raymer, and L. M. Narducci (Cambridge University Press, Cambridge, England, 1986).
[7] *Optical Nonlinearities and Instabilities in Semiconductors,* edited by H. Haug (Academic, Boston, 1988).
[8] Special issue, J. Opt. Soc. Am B **2** (1) (1985).
[9] A. Akhmanov, V. A. Vysloukh, and A. S. Chirkin Usp. Fiz. Nauk **149**, 449 (1986) [Sov. Phys. Usp. **29**, 642 (1986)].
[10] N. I. Zheludev, Usp. Fiz. Nauk **157**, 683 (1989) [Sov. Phys. Usp. **32**, 357 (1989)].
[11] Special issue, J. Opt. Soc. Am. B **7** (6) (1990).
[12] K. Tai. A. Hasegawa, and A. Tomita, Phys. Rev. Lett. **56**, 135 (1986).
[13] G. P. Agrawal, *Nonlinear Fiber Optics* (Academic, Boston, 1989), Sec. 5.1.
[14] V. I. Bespalov and V. I. Talanov, Pis'ma Zh. Eksp. Teor. Fiz. **3**, 471 (1966) [JETP Lett. **3**, 307 (1966)].
[15] G. P. Agrawal, J. Opt. Soc. Am. B **7**, 1072 (1990).
[16] Y. Silberberg and I. Bar-Joseph, J. Opt. Soc. Am B **1**, 662 (1984).
[17] A. L. Gaeta, R. W. Boyd, J. R. Ackerhalt, and P. W. Milonni, Phys. Rev. Lett. **58**, 2432 (1987).
[18] S. A. Akhmanov, M. A. Vorontsov, and V. Yu. Ivanov, Pis'ma Zh. Eksp. Teor. Fiz. **47**, 611 (1988) [JETP Lett. **47**, 707 (1988)].
[19] Y. Silberberg, Opt. Lett. **15**, 1282 (1990).
[20] J. A. C. Heideman and B. M. Herbst, SIAM J. Numer. Anal. **23**, 485 (1986).